CONTROL OF COAXIAL JETS BY AN AZIMUTHAL EXCITATION: VORTEX DYNAMIC AND MIXING PROPERTIES

Guillaume Balarac*, Marcel Lesieur and Olivier Métais
Equipe MoST / LEGI, B.P. 53,
38041 Grenoble Cedex 09, France
guillaume.balarac@hmg.inpg.fr
marcel.lesieur@hmg.inpg.fr
olivier.metais@hmg.inpg.fr

ABSTRACT

The goal of this work is to improve the mixing properties of a coaxial jet with moderate Reynolds number by active control. Two direct numerical simulations of coaxial jets are performed. First, studying a "natural" (without deterministic control) coaxial jet, we show that the appearance of counter-rotating pairs of streamwise vortices allows ejections from the seeding regions. This initiates the turbulent mixing. However spots of unmixed fluids persist at the end of the computational domain. We use then deterministic perturbation to allow an improvement of the mixing properties of the jet. The deterministic perturbation has an azimuthal part which forces the appearance of pairs of streamwise vortices. Finally, we found a real improvement of the mixing properties with a good homogeneity at the end of the computational domain due to a quicker appearance of small scales.

INTRODUCTION

Coaxial jets are composed of an inner jet surrounded by an annular jet. These are present in various industrial applications and are often used as an effective way of mixing two different fluid streams (chemical engineering systems, combustion devices...). The study of mixing properties of coaxial jets has often focused on the near-field because the largest proportion of the mixing takes place in the developing region containing the potential cores (Champagne and Wygnanski, 1971). Moreover, Warda *et al.* (1999) showed that coaxial jets with $r_u > 1$ develop faster than with $r_u < 1$. Consequently, for fixed nozzle configuration, a coaxial jet with high velocity ratio yields rapid mixing between the two jets. As pointed out by Crow and Champagne (1971), the large-scale coherent structures emerging in shear flows play a dominant role in the turbulent transport. Therefore, several authors have focused on the role played by coherent vortices on the mixing in coaxial jets. Villermaux and Rehab (2000) showed that the interface between the two streams increases with the instability of the outer shear layer and so the vorticity thickness of the outer shear layer is an important parameter. As in plane mixing layers (Bernal and Roshko, 1986) and single jets (Liepmann and Gharib, 1992), the coaxial jets develop counter-rotating pairs of streamwise vortices stretched between consecutive vortex rings: these play a major role in the mixing process. A recent numerical study (Balarac *et al.*, 2007) has brought to light the ejections of the species seeded in the outer jet associated to these streamwise vortices. Moreover, this study has investigated the changes in mixing properties implied by the modification of the upstream conditions. The mixing was shown to be improved when the generation of streamwise vortices is favored.

The recent development of Micro Electro Mechanical System (MEMS) makes possible new ways of controlling the coaxial jets (Angele *et al.*, 2006). These works show that a non-axisymmetric forcing (based on micro flap actuators) allows a faster development of the streamwise vortices, and they observe that this forcing leads to mixing enhancement. In these studies, the forcing was applied only on the outer shear layer because of its domination on the jet dynamics. Indeed, Dahm *et al.* (1992) found that the vortical motion is dominated by the vortices emerging in the outer shear layer when the annular flow velocity is larger than the central one. In fact, Balarac and Métais (2004) showed that the vortices of the outer shear layer develop with a Strouhal number corresponding to the value predicted by the linear stability theory for the Kelvin-Helmholtz instability of this shear layer. Conversely, they found that the inner vortices are trapped in the free space between two consecutive outer vortices. The inner vortices evolution is thus dictated by the outer vortices motion: it is the "locking" phenomenon. Thus, large-scale structure modifications, especially in the outer mixing layer, have a large effect on the mixing properties of coaxial jets. Similarly, in the present work, we manipulate the jet outer vortices generation to obtain mixing enhancement: we thus impose a deterministic perturbation at the inlet. We here use direct numerical simulations (DNS).

NUMERICAL METHOD

Our numerical code solves the constant density Navier-Stokes equations written in Cartesian coordinates using a mixed pseudo-spectral scheme in the two transverse direction taken as periodic and a sixth-order-compact scheme in the streamwise direction. The time advancement is assured by a third order Runge-Kutta scheme and pressure velocity coupling is modelled by a fractional field. The mixing is studied by considering the mixture fraction, f, of the species seeded within the outer annular jet at the jet inlet. Thus, $f = 1$ (resp. 0) if there are only species seeded in the outer annular at the inlet (resp. if there are only species seeded in the remainder of the upstream jet: the inner jet and the coflow). The mixture fraction evolution is given by a transport equation (convection-diffusion) which is solved simultaneously with the Navier-Stokes equations. For the spatial discretization of the convection term, we use a second-order semi-discretized TVD Roe scheme.

Following the streamwise direction, the outlet boundary

*present address: CTR, Stanford University, Stanford, CA 94305, USA. balarac@stanford.edu condition uses a non-reflective condition and the inlet condition is given by a velocity profile with the shape:

$$\vec{U}(\vec{x}_0,t) = \vec{U}_{coax}(\vec{x}_0) + \vec{U}_{noise}(\vec{x}_0,t) + \vec{U}_{forc}(\vec{x}_0,t). \quad (1)$$

$\vec{U}_{coax}(\vec{x}_0) = (U_{coax}(\vec{x}_0),0,0)$ mimics a realistic experimental profile of coaxial jets. $U_{coax}(\vec{x}_0)$ is constructed by two hyperbolic tangent profiles:

$$U_{coax}(\vec{x}_0 = (0,r,\phi)) = \begin{cases} \frac{U_1+U_2}{2} + \frac{U_1-U_2}{2}\tanh\left(\frac{r-R_1}{2\theta_{01}}\right) \\ \text{for} \quad r < R_m \\ \\ \frac{U_2+U_3}{2} + \frac{U_2-U_3}{2}\tanh\left(\frac{r-R_2}{2\theta_{02}}\right) \\ \text{for} \quad r > R_m \end{cases} \quad (2)$$

In Eq. (2), U_1, U_2 and U_3 are the inner jet, the outer jet and the coflow velocities respectively. Moreover, R_1, R_2 and $R_m = (R_1+R_2)/2$ are the inner, the outer and the averaged radii, and θ_{01} and θ_{02} the inlet momentum thicknesses of the inner and outer shear layers (see figure 1). The inlet

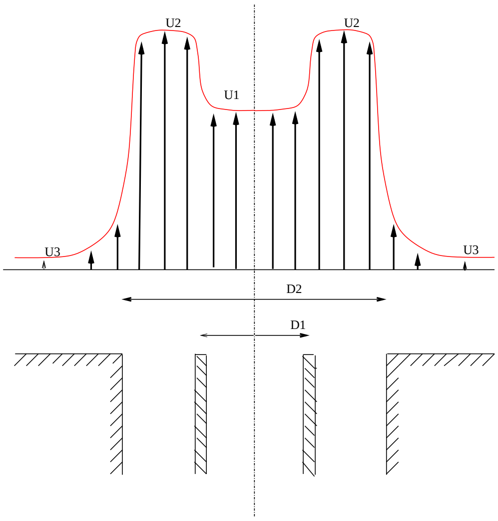

Figure 1: Sketch of the inlet velocity profile.

mixture fraction profile is also built with hyperbolic tangents (Balarac *et al.*, 2007). We prescribed $f = 1$ in the outer annular jet and $f = 0$ in the remainder of the flow. In eq.(1), $\vec{U}_{noise}(\vec{x}_0,t)$ is a noise superimposed on the inlet profile. It is given by

$$\vec{U}_{noise}(\vec{x}_0,t) = AU_{base}(\vec{x}_0)\vec{f}, \quad (3)$$

where A is the maximum amplitude of the incoming noise limited to $A = 3\%$. The noise is mainly located in the inner and outer shear layers by the $U_{base}(\vec{x}_0)$ function:

$$U_{base}(\vec{x_0}) = \begin{cases} 0.5 & \text{if} \quad 0.85 > r/R_1 \\ 1.0 & \text{if} \quad 0.85 < r/R_1 < 1.15 \\ 1.0 & \text{if} \quad 0.85 < r/R_2 < 1.15 \\ 0 & \text{otherwise.} \end{cases}$$

In equation (3), $\vec{f}$ is a random noise applied in the three directions and designed to satisfy a given energy spectrum. Note that the noise is imposed on the three velocity components. More details about the inlet mean velocity profile and the noise in coaxial jets can be found in da Silva *et al.* (2003). Note that this numerical code has been previously used in several studies of plane jet (da Silva and Métais, 2002a), round jet (da Silva and Métais, 2002b) and coaxial jet (Balarac and Métais, 2005; Balarac *et al.*, 2007). Finally, $\vec{U}_{forc}(\vec{x}_0,t)$ defines the deterministic perturbation imposed to excite the jet.

In this work, two simulations are performed. First, we take $\vec{U}_{forc}(\vec{x}_0,t) = 0$ to have a reference case to which the forced case can be compared. The forced case is defined to minimize the addition of energy at the inlet. Thus the excitation is applied only in the outer shear layer and with a moderate amplitude. Moreover, the excitation is performed at the preferential frequency of the outer shear layer f_o and it is defined to be always positive. This corresponds to pure blowing without aspiration which is more realistic as far as practical applications are concerned. Finally, we take

$$\begin{aligned} U_{forc}(\vec{x}_0,t) = \quad & \epsilon U_{loc}(\vec{x}_0)(1/2 + 1/2\sin(2\pi f_o t)) \\ & \times(1/2 + 1/2\sin(5\phi)). \end{aligned} \quad (4)$$

In this equation, $U_{loc}(\vec{x}_0)$ is a function aimed to localize the excitation only in the outer shear layer, the maximum amplitude is fixed by ϵ and is equal at 8% of U_2. The last term in eq.(4) is the azimuthal part of the forcing with an azimuthal wave number equal to 5. The forcing is not an axisymmetric forcing and its main goal is to allow the early generation of streamwise vortices. In fact, this excitation mimics the role played by 5 micro-jets placed circumferentially around the outer diameter and blowing with a frequency equals to f_o. A sketch of this excitation is given by the figure 2.

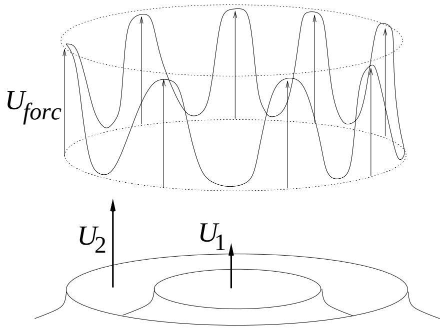

Figure 2: Sketch of the azimuthal excitation with an azimuthal waves number equal to 8.

The flow and computational parameters are then the following for both simulations. The domain size is $10.8D_1 \times 10.65D_1 \times 10.65D_1$ along the streamwise (x) and the two transverse directions (y,z). D_1 is the inner diameter. $231 \times 384 \times 384$ grid points with uniform mesh size are used. The upstream mean velocity profile is defined with a velocity ratio ($r_u = U_2/U_1$) equals to 5 and a diameter ratio ($\beta = D_2/D_1$) equals to 2. The initial momentum thicknesses are defined with $D_1/\theta_{01} = D_1/\theta_{02} = 25$. Finally, the Reynolds number based on the outer jet velocity and the inner jet diameter is $Re = U_2D_1/\nu = 3000$ and the Schmidt number is taken equal to 1.

GLOBAL VIEW OF UNFORCED JET

To have a reference case to properly compare the forced case, we perform a simulation of a coaxial jet with the same parameters but with $U_{forc} = 0$. This jet is without deterministic perturbation. There is just a weak "white noise" to allow a natural transition toward a developed turbulence state and we so refer to this jet as the "natural" jet. To understand the modification due to the deterministic perturbation, we summarizes some of the results previously obtained by Balarac *et al.* (2007) for this natural coaxial jet.

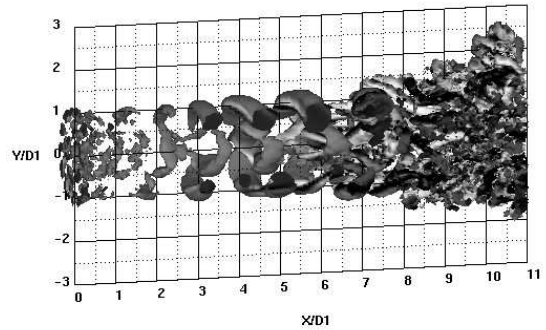

Figure 3: Coherent vortices for the unforced coaxial jet shown by isosurface of $Q = 0.5(U_2/D_1)^2$ colored by the streamwise vorticity (light grey: negative values; dark grey: positive values). A part of the outer rings is artificially cut to show the inner rings.

The figure 3 shows an isosurface of positive Q colored by the streamwise vorticity. Q is the second invariant of the velocity gradient tensor. The positive Q criterion has been proposed by Hunt *et al.* (1988) and it is now known as a good indicator of the coherent vortices. The figure 3 shows so the vortex dynamic during the transition of the jet. First, the Kelvin-Helmholtz instability disturbs the shear layers and leads to the Kelvin-Helmholtz rings formation. Due to the upstream mean velocity shape, there are two types of Kelvin-Helmholtz vortices created: between the inner jet and the annular jet and between the annular jet and the coflow. These two types turn in opposite sense. The figure shows that the space between two consecutive Kelvin-Helmholtz rings on the inner shear layer are the same that between two consecutive outer rings. It is due to the "locking" phenomenon which allow to the outer rings to impose their motion at the inner rings (Balarac and Métais, 2004). After $x/D_1 \approx 6$, the second step of the transition is the appearance of pairs of counter-rotating streamwise vortices. These vortices appear between two consecutive rings and they are due to secondary instability of the free shear layer. This step leads to an important longitudinal stretching phenomenon which allows the three-dimensionalization of the flow (Balarac and Métais, 2005). Further downstream, just before the end of the computational domain, the growth of the small scale turbulence as well as the breakdown of the large scale cohrent structures makes their identification very difficult. Finally, the flow reaches a fully turbulent state since the frequency spectra has a well defined $-5/3$ range over about one decade (Balarac *et al.*, 2007).

Figure 4 shows the evolution of the mixture fraction, f, in the central plane of the unforced jet. After a region only dominated by a molecular diffusion ($0 < x/D_1 < 4$), the turbulent mixing develops thanks to coherent vortices. First, the Kelvin-Helmholtz vortices allow an engulfment of the species seeded in the annular jet towards the inner and outer shear layers. After ($x/D_1 > 6$), the counter-rotating streamwise vortices appearance imply ejections of the species seeded in the outer annular jet. These ejections allow for the inter-penetration of both streams and really initiate the turbulent mixing. The sudden increase of the rms mixture fraction, $\langle f'^2 \rangle^{1/2}$ corresponds thus with the growth

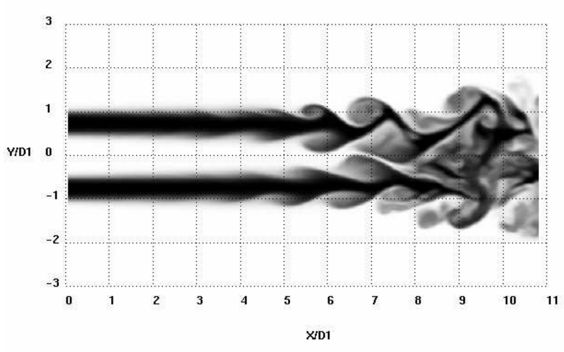

Figure 4: Instantaneous contours of the mixture fraction in the central plane of the unforced jet. f varies from 0 (white) to 1 (black).

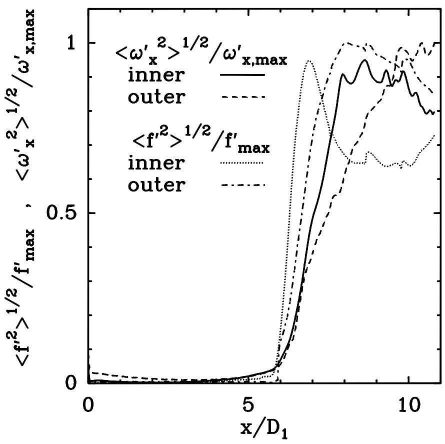

Figure 5: Downstream evolution of the rms streamwise vorticity and the rms mixture fraction in both inner and outer jets in the unforced jet. Each rms quantities is normalized by its maximum rms value.

of the rms axial vorticity $\langle \omega_x'^2 \rangle^{1/2}$ due to the streamwise vortices emergence (Fig.5). At the end of the transition, large amount of species seeded in the upstream annular jet invade the center of the jet. Moreover the inner and outer mixing layers merge in order to create a single mixing zone similar to a single jet. In this region, the turbulent scale undergo an intense turbulent mixing however spots of unmixed fluid persist. This appear clearly on the mixture fraction PDF at the end of the computational domain (Fig.6). Indeed, there are high probabilities to find $f = 1$ close to the jet center. Moreover, a non-marching PDF is found. A non-marching PDF is characterized by a most probable value of f quasi-independent of the radial position and distinct from the mean value. This shape is produced by the persistence of large-scale mixing. Conversely, a marching PDF is the signature of small-scale mixing and this is characterized by a most probable value equals to the mean value (Pickett and Ghandhi, 2002). The PDF shape found reveals that the mixing is not homogeneous in this region. In the following sections, the deterministic perturbation is added to obtain a better mixing efficiency at the end of the computational domain. First, the flow dynamic modifications are studied.

FLOW DYNAMIC OF THE FORCED JET

Here, we investigate the flow dynamic of a coaxial jets under the excitation given by the equation (4). First, an instantaneous view of coherent vortices is displayed in fig-

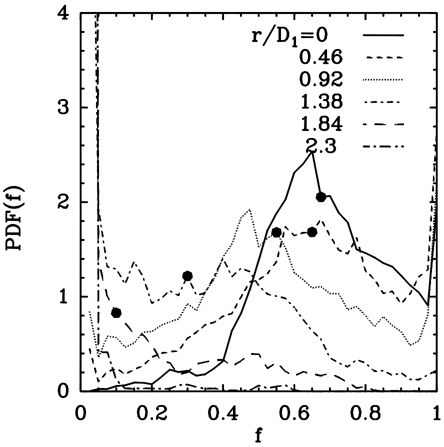

Figure 6: Mixture fraction PDF across the mixing layer at $x/D_1 = 10$. The points show the mean value of f for each radial location.

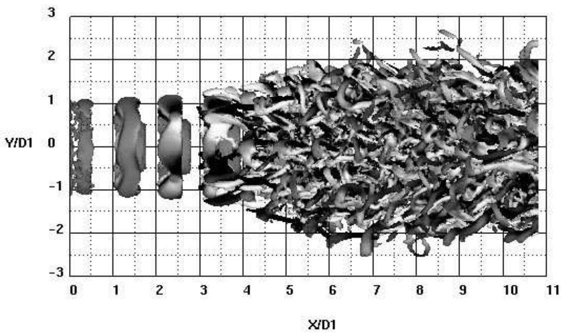

Figure 7: Coherent vortices for the forced coaxial jet shown by isosurface of $Q = 0.5(U_2/D_1)^2$ colored by the streamwise vorticity (light grey: negative values; dark grey: positive values).

ure 7. We can see that there is a rapid amplification of the Kelvin-Helmholtz instability on the outer shear layer. This is due to the temporal part of the forcing which disturbs the outer shear layer with the preferential frequency of this shear layer. Thus, the outer Kelvin-Helmholtz rings are well formed from the beginning of the jet. The figure 8 shows that the Kelvin-Helmholtz vortices on the inner shear layer (which is not forced) appear also sooner than in the unforced case. This is due to the "locking" phenomenon. Indeed, there is a dynamical domination of the outer vortices which imposes their motion to the inner ones. However, opposed to a purely axisymmetric forcing, the outer rings do not exhibit an axisymmetric shape. Indeed, the azimuthal part of the forcing leads to an azimuthal deformation of the tori. Note that the inner rings stay axisymmetric (without azimuthal deformation) conversely to the outer ones (Fig.8). If the outer shear layer controls the generation of the inner Kelvin-Helmholtz instability, it does not seem that the outer rings influence the inner rings as far as the azimuthal instabilities are concerned. Finally, the azimuthal disturbance leads to the quick appearance of 5 pairs of counter-rotating streamwise vortices corresponding to the value of the azimuthal wave number. This appearance is quickly followed by the formation of small turbulent structures and the flow becomes turbulent.

A better comprehension of the flow dynamic modification can be obtained by the study of the radial and azimuthal

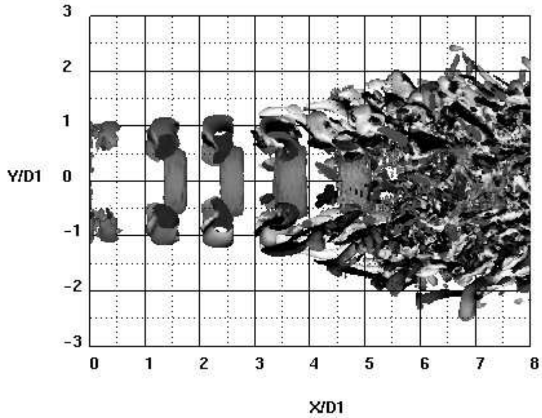

Figure 8: Zoom of coherent vortices for the forced coaxial jet shown by isosurface of $Q = 0.5(U_2/D_1)^2$ colored by the streamwise vorticity (light grey: negative values; dark grey: positive values). Large part of the outer vortices are artificially cut to see the inner ones.

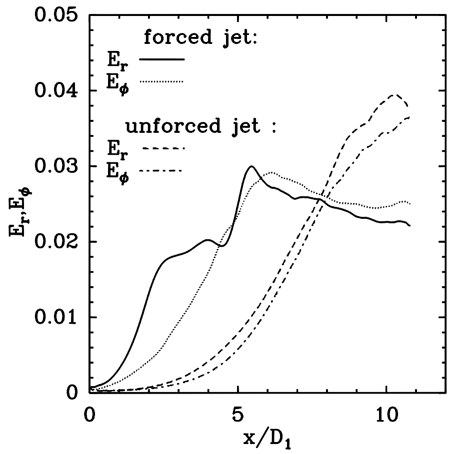

Figure 9: Downstream evolution of the radial and azimuthal contributions to the turbulent kinetic energy calculated in the outer shear layer - Eq.(7) and (8). Comparison between the unforced and the forced jets.

Reynolds stresses contributions to the turbulent kinetic energy. Thus da Silva *et al.* (2003) defined the quantities E_r and E_ϕ by

$$E_r(x) = \sqrt{\frac{2\pi}{L_y L_z}\int_0^{R_m} \langle u_r'^2 \rangle (x,r) r dr}, \tag{5}$$

$$E_\phi(x) = \sqrt{\frac{2\pi}{L_y L_z}\int_0^{R_m} \langle u_\phi'^2 \rangle (x,r) r dr}, \tag{6}$$

for the inner shear layer and by

$$E_r(x) = \sqrt{\frac{2\pi}{L_y L_z}\int_{R_m}^{\infty} \langle u_r'^2 \rangle (x,r) r dr}, \tag{7}$$

$$E_\phi(x) = \sqrt{\frac{2\pi}{L_y L_z}\int_{R_m}^{\infty} \langle u_\phi'^2 \rangle (x,r) r dr}. \tag{8}$$

for the outer shear layer, respectively. Note that in these equations, u_r' and u_ϕ' are the radial and the azimuthal

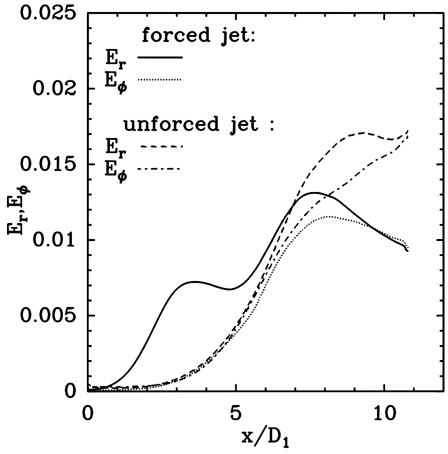

Figure 10: Downstream evolution of the radial and azimuthal contributions to the turbulent kinetic energy calculated in the inner shear layer - Eq.(5) and (6). Comparison between the unforced and the forced jets.

component of the fluctuating velocity. E_r is linked to the development of the Kelvin-Helmholtz instabilities and the growth of the vortex rings whereas E_ϕ, associated with the azimuthal instabilities, constitutes a measure of the three-dimensionality level. On the outer shear layer (Fig.9), we can see that the quantities E_r and E_ϕ begin to grow earlier in the forced case than in the natural jet. Moreover, in the first transition stage, the main contribution to the turbulent kinetic energy comes from the radial component and E_ϕ begin to grow latter. This is consistent with the flow visualization where we can see that the azimuthal deformation of the outer rings grows in the beginning of the transition. Finally, E_ϕ has a significant contribution from $x/D_1 = 4$ corresponding with the streamwise vortices emergence. For the inner shear layer, figure 10 shows that E_r grows also earlier in the forced case, but E_ϕ keeps a behaviour very close to the natural case during the transition. This confirms that the inner shear layer is influenced by the outer Kelvin-Helmholtz instabilities but it is not influenced by the azimuthal disturbance imposed on the outer shear layer. This is consistent with the axisymmetric persistence of the inner Kelvin-Helmholtz rings found above (Fig.8). Finally, we can note that in the forced case, at the end of the computational domain, there is $E_r \approx E_\phi$ showing a three-dimensionalization of the jet.

MIXING PROPERTIES OF THE FORCED JET

The mixing properties of the jet are also greatly influenced by the deterministic forcing. Indeed, figure 11 displays contours of the mixture fraction in the central plane of the forced jet. The main mixing stages can be viewed. First, the region dominated by the molecular diffusion is shorter in this case as compared with the unforced case (Fig.4). This is due to the temporal part of the forcing which allows a quicker appearance of the Kelvin-Helmholtz rings implying a rapid engulfment of the outer stream towards the inner and the outer mixing layer. After $x/D_1 = 4$, the streamwise vortices appearance allows an intense ejection phenomenon. Figure 12 shows contours of the mixture fraction in a transverse section. The ejection phenomenon is characterized by the mushroom-type structures. Conversely to the natural jet, these mushroom-type structures are well formed and the number of these structures is dependent of the azimuthal

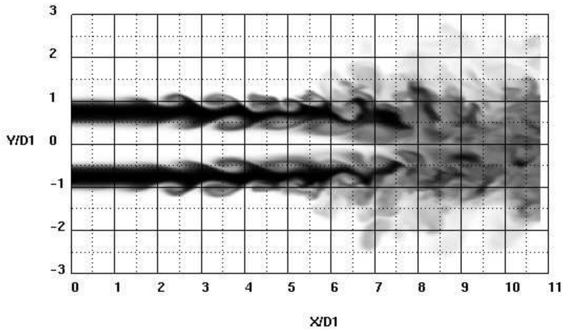

Figure 11: Instantaneous contours of the mixture fraction in the central plane of the forced jet. f varies from 0 (white) to 1 (black).

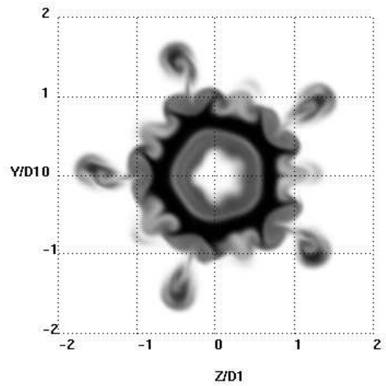

Figure 12: Instantaneous contours of the mixture fraction in a transverse section ($x/D_1 = 4.5$) for the forced jet. f varies from 0 (white) to 1 (black).

wavenumber of the deterministic forcing. At the end of the computational domain, the flow reaches a fully-turbulent state and the small-scales appearance leads to a homogenous mixing without spot of unmixed fluid conversely to the unforced case.

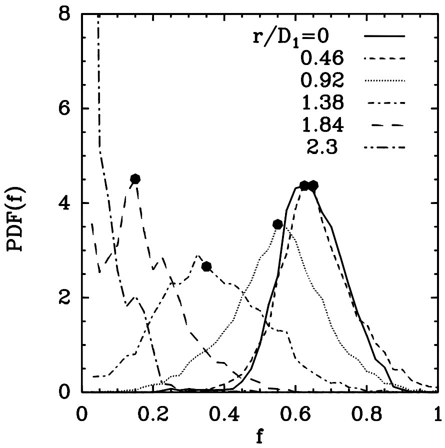

Figure 13: Mixture fraction PDF across the mixing layer at $x/D_1 = 10$. The points show the mean value of f for each radial location.

A better comparison of the mixing state between the forced and the unforced case can be given by the mixture fraction PDF. Figure 13 shows the mixture fraction PDF of the shear layer at $x/D_1 = 10$. In this case, a marching-type PDF is found since the most probable value of f corresponds to the mean value at each radial location. This indicates a small-scale mixing conversely to the unforced case. Moreover, there is no probability to find spots of unmixed species, $f = 1$ contrary to the unforced case. This indicates a real mixing improvement due to the deterministic perturbation.

CONCLUSION

The goal of the present study was to find appropriate deterministic perturbation to control coaxial jets at moderate Reynolds number to improve their mixing properties. The forced jet dynamics and mixing properties are compared with a "natural" jet recently studied in details by Balarac *et al.* (2007). For the natural jet, the beginning of the transition is due to the appearance of Kelvin-Helmholtz rings on the inner and outer shear layers. There is a domination of the outer Kelvin-Helmholtz vortices which impose their motion to the inner ones. For the mixing process, this stage allows an engulfment of the species seeded in the annular jet towards the inner and the outer mixing layer. Further downstream, counter-rotating pairs of streamwise vortices appear between two consecutive Kelvin-Helmholtz rings. This allow to eject outer species. These ejections are characterized by mushroom-type structures and they play a dominant role in the mixing process. However, spots of unmixed fluid are found at the end of the transition in the unforced case showing that there is not yet a homogenous mixing. We have then used a deterministic perturbation to improve the mixing.

This perturbation is applied only on the outer shear layer because of the outer vortices domination on the flow dynamic. Moreover, the perturbation consists of a combination between a temporal part and an azimuthal part with an azimuthal wave number equals to 5. The temporal part allows to disturb the outer shear layer with its preferential frequency and the azimuthal part allows to give an azimuthal deformation of the outer Kelvin-Helmholtz vortices. In fact this perturbation mimics the role played by 5 microjets placed circumferentially around the outer nozzle and ejecting periodically. This perturbation allows a rapid development of the outer and inner Kelvin-Helmholtz vortices implying an efficient engulfment of the outer species. Moreover, the azimuthal deformation of the outer Kelvin-Helmholtz vortices leads to the early formation of counter-rotating streamwise vortices. These streamwise vortices are more intense and they allow to generate intense ejection of the species seeded in the outer jet. Note that the outer Kelvin-Helmholtz instabilities disturb the inner shear layer but that the outer azimuthal instabilities seem not influenced the inner shear layer and the inner Kelvin-Helmholtz vortices keep their axisymmetry. Finally, the mixing is more homogenous without spot of unmixed fluid in the forced case conversely to the "natural" case. This show a real improvement of the mixing efficiency due to the deterministic perturbation

REFERENCES

Angele, K., Kurimoto, N., Suzuki, Y., and Kasagi, N., 2006, "Evolution of the streamwise vortices in coaxial jet controlled with micro flap actuators", *J. of Turbulence*, 7(73):1-19.

Balarac, G., and Métais, O., 2004, "Coherent vortices in coaxial jets", *Advances in Turbulence X*, H.I. Anderson and P.-Å. Krogstad editors (CIMNE, Barcelona).

Balarac, G., and Métais, O., 2005, "The near field of coaxial jets : A numerical study", *Phys. Fluids*, 17 (065102):1-14.

Balarac, G., Si-Ameur, M., Lesieur, M., and Métais, O., 2007, "Direct numerical simulations of high velocity ratio coaxial jets: Mixing properties and influence of the upstream conditions", *J. of Turbulence*, 8(21):1-27.

Bernal, L. P., and Roshko, A., 1986, "Streamwise vortex structure in plane mixing layers", *J. Fluid Mech.*, 170:449-525.

Champagne, F. H., and Wygnanski, I. J., 1971, "An experimental investigation of coaxial turbulent jets", *Int. J. Heat Mass Transfer*, 14:1445-1464.

Crow, S. C., and Champagne, F. H., 1971, "Orderly structure in jet turbulence", *J. Fluid Mech.*, 48:547-591.

Dahm, W. J. A., Frieler, C. E., and Tryggvason, G., 1992, "Vortex structure and dynamics in the near field of a coaxial jet", *J. Fluid Mech.*, 241:371-402.

Hunt, J. C. R., Wray, A. A., and Moin, P., 1988 "Eddies, stream, and convergence zones in turbulent flows" *Annual Research Briefs*, CTR, Stanford University.

Liepmann, D., and Gharib., M., 1992, "The role of the streamwise vorticity in the near-field entrainment of a round jet", *J. Fluid Mech.*, 245:643-668.

Pickett, L. M., and Ghandhi, J. B., 2002, "Passive scalar mixing in a planar shear layer with laminar and turbulent inlet conditions", *Phys. Fluids*, 14(3):985-998.

da Silva, C. B., Balarac, G., and Métais, O., 2003, "Transition in high velocity ratio coaxial jets analysed from direct numerical simulations", *J. of Turbulence*, 4(24):1-18.

da Silva, C. B., and Métais O., 2002a, "On the influence of coherent structures upon interscale interactions in turbulent plane jets", *J. Fluid Mech.*, 473:103-145.

da Silva, C. B., and Métais O., 2002b, "Vortex control of bifurcating jets: a numerical study", *Phys. Fluids*, 14(11):3798-3819.

Villermaux, E., and Rehab, H., 2000, "Mixing in coaxial jets", *J. Fluid Mech.*, 425:161-185.

Warda, H. A., Kassab, S. Z., Elshorbagy, K. A., and Elsaadawy, E. A., 1999, "An experimental investigation of the near-field region of a free turbulent coaxial jet using LDA", *Flow Measurement and Instrumentation*, 10:15-26.